CHEMISTRY OF MATERIALS
Article

Chem. Mater. **2010,** *22,* 541–550 541
DOI:10.1021/cm903516t

Synthesis, Structural Characterization, and Properties of Perovskites Belonging to the xBiMnO$_3$−(1 − x) PbTiO$_3$ System

Alicia Castro,* Eladio Vila, Ricardo Jiménez, Jorge Hernández-Velasco, Teresa Hungría, and Miguel Algueró

Instituto de Ciencia de Materiales de Madrid, CSIC, Cantoblanco, 28049 Madrid, Spain

Received November 19, 2009

The xBiMnO$_3$−(1 − x) PbTiO$_3$ solid solution has been synthesized by an accurate, nonclassical, wet-chemistry method. Results show the existence of two structurally different perovskites, depending on the x value: tetragonal for $0 \leq x < 0.36$; pseudocubic for $0.44 < x \leq 0.8$; and a morphotropic phase boundary (MPB) between both symmetries for $0.36 \leq x \leq 0.44$. When $x \geq 0.76$, unidentified diffraction lines appear together with those of the perovskite. The evolution of the unit-cell parameters has been studied by X-ray diffraction techniques. The stability of different symmetries can be correlated with the Goldschmidt's tolerance factors (t) for perovskites, with the MPB only existing for a critical $t \approx 1.00$ value. Materials with $x \leq 0.4$ exhibit the ferroelectric transition above room temperature; their Curie temperatures have been determined by thermal analysis, dielectric versus temperature measurements, and dynamical−mechanical analysis. This temperature decreases as the bismuth and manganese contents increase, being as low as Tc = 446 K for $x = 0.4$. Elastic properties also suggest the existence of a second low temperature transition to a nonferroelastic phase, in which temperature increases with x. Trends of the two transitions point to the existence of a critical composition above which a ferroelectric transition does not occur, in coincidence with the limit of the tetragonal phase and the end of the MPB region. Moreover, magnetic interactions have also been detected at low temperature in $x \geq 0.2$ samples.

Introduction

Ferroelectric materials derived from PbTiO$_3$ are widely used as active elements of piezoelectric devices, mainly solid solutions of the tetragonal perovskite with one of different symmetry, for example orthorhombic PbZrO$_3$,[1] with compositions belonging to a morphotropic phase boundary between tetragonal and rhombohedral polymorphs. However, the environmental aggressiveness of lead in these oxides has suggested the research of new lead-free or lead-less materials. Bismuth-containing perovskites and particularly the solid solutions BiBO$_3$−PbTiO$_3$ (B = transition metals)[2−7] have been considered as substitutes for nowadays commercial piezoelectric materials. In fact, Bi^{3+} and Pb^{2+} cations, occupying the A site of perovskite, exhibit a very similar stereochemical behavior, due to the presence of their 6s^2 active lone-pair of electrons,[8] which opens the possibility of aliovalent substitutions of Bi^{3+} for Pb^{2+}, maintaining the basal perovskite network.

On the other hand, in the last ten years, the study and the search for new multiferroic materials has been another major challenge, due to their potential applications in electronic technology. Multiferroics are materials that simultaneously exhibit two or three primary ferroic properties (ferroelasticity, ferro- or antiferromagnetism, and ferroelectricity) in one single and homogeneous phase, but the most technologically promising materials are those showing the coupling between both ferroelectric and magnetic order parameters, this is the magnetoelectrics.

In this way, while the parent piezoelectric material can be considered PbTiO$_3$, BiFeO$_3$ probably is the most studied multiferroic material,[9] perhaps because it is the only known oxide that is antiferomagnetic and ferroelectric at room temperature. Nevertheless, there are other perovskite oxides under consideration, such as BiMnO$_3$ that is also a very good magnetoelectric candidate. This oxide is the only among BiBO$_3$ thought to exhibit proper ferroelectric and ferromagnetic behavior, properties believed to arise from the 6s^2 lone pair and

*To whom correspondence should be addressed. Tel: +34 913349000. Fax: +34 913720623. E-mail: acastro@icmm.csic.es.

(1) Cross, L. E. *Nature* **2004**, *432*, 24.
(2) Eitel, R. E.; Randall, C. A.; Shrout, T. R.; Park, S. E. Jpn. J. Appl. Phys. Part 1, **2002**, *41*, 2099.
(3) Randall, C. A.; Eitel, R.; Jones, B.; Shrout, T. R.; Woodward, D. I.; Reaney, I. M. *J. Appl. Phys.* **2004**, *95*, 3633.
(4) Suchomel, M. R.; Davies, P. K. *J. Appl. Phys.* **2004**, *96*, 4405.
(5) Choi, S. M.; Stringer, C. J.; Shrout, T. R.; Randall, C. A. *J. Appl. Phys.* **2005**, *98*, 034108.
(6) Khalyavin, D. D.; Salak, A. N.; Vyshatko, N. P.; Lopes, A. B.; Olekhnovich, N. M.; Pushkarev, A. V.; Maroz, I. I.; Radyush, Y. V. *Chem. Mater.* **2006**, *18*, 5104.
(7) Algueró, M.; Ricote, J.; Hungría, T.; Castro, A. *Chem. Mater.* **2007**, *19*, 4982.
(8) Galy, J.; Meunier, G.; Andersson, S.; Aström, A. *J. Solid State Chem.* **1975**, *13*, 142.
(9) Catalan, G.; Scott, J. F. Adv. Mater. **2009**, *21*, 2463; and references therein.

Published on Web 12/10/2009

orbital ordering.[10−12] $BiMnO_3$ seems to crystallize at room temperature as a highly-distorted perovskite structure, in the noncentrosymmetric *C2* (No. 5) monoclinic space group[13,14] and undergoes two high-temperature transitions at 474 K, monoclinic−monoclinic, and at 768 K, monoclinic−orthorhombic (*Pbmn*, No. 53), which has been associated to the ferro-paraelectric transition.[15−17] It also presents a ferromagnetic transition at about 100 K, temperature around which a fairly large magnetocapacitance effect is found that is consistent with magnetoelectric coupling.[17]

From the point of view of synthesis, only a few of the possible bismuth-containing perovskites can be prepared by conventional methods but at high pressure. This fact could be attributed to the smaller Bi^{3+} ionic radius, in comparison with that of Pb^{2+} (ionic radii in cuboctahedral coordination: $rBi^{3+} = 1.34$ Å, $rPb^{2+} = 1.49$ Å),[18] giving rise to very low tolerance factors. This is particularly true for multiferroic perovskites, where scarce phases can be prepared at room pressure, for example $BiFeO_3$, while $BiMnO_3$ can only be synthesized after a high-pressure and high-temperature reaction.

A lot of work has been done in order to obtain new materials, classically belonging to $BiBO_3$−$PbTiO_3$ binary systems, with a triple aim: to diminish the Pb content in piezoelectric materials, maintaining or even enhancing their properties, for example in high-sensitivity piezoelectric materials (B = Sc, Mg, Zn, Ga,. . .);[2−7,19] to stabilize low tolerance factor perovskites;[7] and finally, to search for new multiferroic and more exact magnetoelectric materials, being B a magnetically active cation, like Fe^{3+} or Mn^{3+}.[15,20−24]

To the best knowledge of the authors, only one paper has been published dealing with the $x$$BiMnO_3$−$(1 - x)$ $PbTiO_3$ system.[23] In this work, the preparation of ceramics with different compositions, ranging between $0 < x \leq 0.7$, is reported. The authors claim the existence of two crystallographic forms, depending on the composition: pseudocubic for $0.7 > x > 0.4$ and tetragonal, isostructural to $PbTiO_3$ for $x < 0.4$. Unlike in the $x$$BiFeO_3$−$(1 - x)$ $PbTiO_3$ system,[20] these authors do not report the existence of a morphotropic phase boundary but a frustration between different preferred environments of cations for $x > 0.4$, which leads to the absence of long-range ordered polar ionic displacements and so to the pseudocubic structure. The permittivity versus temperature measurements reported in the same work, seem to reveal a clear ferro-paraelectric transition at about 730 K for $x = 0.2$, and relaxor-like behavior for $x = 0.3$ and 0.4 samples, which support the proposed frustration phenomenon.

This work deals with the synthesis of the $x$$BiMnO_3$−$(1 - x)$ $PbTiO_3$ solid solution, by the use of an accurate and nonclassical wet-chemistry method, as well as the processing of high-quality-ceramic materials by a conventional sintering technique. This system has been studied from the point of view of their structural characteristics and physical properties. It is worth noting the existence of a quite wide morphotropic phase boundary, between tetragonal and cubic symmetries, for compositions close to $x \approx 0.4$.

The Curie temperature of ferroelectric phases has been determined by differential thermal analysis and dielectric measurement as a function of the temperature, for x value up to 0.25. From this value up to $x = 0.4$, the Curie temperature has been determined by dynamical mechanical analysis. These results allow us to confirm that $x$$BiMnO_3$−$(1 - x)$ $PbTiO_3$ maintains the ferroelectric phase up to $x = 0.4$ and to discuss its disappearance beyond this value.

Finally, magnetic measurements have also been carried out on samples with $0.1 \leq x \leq 0.6$, showing the existence of ferromagnetic interactions at low temperature (< 50 K).

Experimental Section

Synthesis and Ceramic Processing. An original wet-chemistry method has been employed for the synthesis of reactive precursors of $x$$BiMnO_3$−$(1-x)$ $PbTiO_3$ (hereafter xBM−PT) phases. These precursors were prepared by adding the amount of TiO_2 required to obtain a Bi−Mn−Pb−Ti molar ratio of x:x:$(1 - x)$:$(1 - x)$ to $0.03x$ mol of $Bi(NO_3)_3 \cdot 5H_2O$, $0.03x$ mol of $Mn(NO_3)_2 \cdot 4H_2O$, and $0.03\ (1 - x)$ mol of PbO, all of them dissolved in 10 ml of HNO_3 (65% concentration), to which 200 mL of distilled water was added, under continuous stirring. The precursor powders were obtained by precipitation of bismuth, manganese, and lead cations with dropwise addition ($2\ mL \cdot min^{-1}$) of 1 M solution of *n*-butylamine up to pH ≈ 9.5, under vigorous stirring. Then, the resultant suspension was filtered, and the precipitate was dried at 353 K. The solid precursors were annealed at 923 K for burning out water, nitrates, and organic ions; this treatment allows the synthesis of xBM−PT to be started, particularly for low x values. Finally, powdered samples were uniaxially pressed into 12 mm diameter disks and further heated in air up to 1273 K for $x \leq 0.6$ and to 1223 K for $0.6 < x \leq 0.8$, for 2 hours. Well sintered ceramics were obtained with relative densities of about 95%.

Similar results were obtained when solid Mn_2O_3 was added with TiO_2 to the $Bi(NO_3)_3 \cdot 5H_2O$ and PbO solution.

(10) Ramesh, R.; Spaldin, N. A. *Nat. Mater.* **2007**, *6*, 21.
(11) Eerenstein, W.; Mathur, N. D.; Scott, J. F. *Nature* **2006**, *442*, 759.
(12) Seshadri, R.; Hill, N. A. *Chem. Mater.* **2001**, *13*, 2892.
(13) Yokosawa, T.; Belik, A. A.; Asaka, T.; Kimoto, K.; Takayama-Muromachi, E.; Matsui, Y. *Phys. Rev. B* **2008**, *77*, 024111.
(14) Kodama, K.; Iikubo, S.; Shamoto, S.; Belik, A. A.; Takayama-Muromachi, E. *J. Phys. Soc. Jpn.* **2007**, *76*, 124605.
(15) Belik, A. A.; Kato, K.; Takayama-Muromachi, E. *J. Solid State Chem.* **2009**, *182*, 685.
(16) Belik, A. A.; Iikubo, S.; Yokosawa, T.; Kodama, K.; Igawa, N.; Shamoto, S.; Azuma, M.; Takano, M.; Kimoto, K.; Matsui, Y.; Takayama-Muromachi, E. *J. Am. Chem. Soc.* **2007**, *129*, 971.
(17) Kimura, T.; Kawamoto, S.; Yamada, I.; Azuma, M.; Takano, M.; Tokura, Y. Phys. Rev. B **2003**, *67*, 180401(R).
(18) Shannon, R. D. *Acta Crystallogr.* **1976**, *A32*, 751.
(19) Cheng, J. R; Zhu, W.; Li, N.; Cross, L. E. *Mater. Lett.* **2003**, *57*, 2090.
(20) Bhattacharjee, S.; Tripathi, S.; Pandey, D. *Appl. Phys. Lett.* **2007**, *91*, 042903.
(21) Yan, F.; Sterianou, I.; Miao, S.; Reaney, I. M.; Lai, M. O.; Lu, L. *J. Appl. Phys.* **2009**, *105*, 074101.
(22) Selbach, S. M.; Tybell, Th.; Einarsrud, M. A.; Grande, T. *Phys. Rev. B* **2009**, *79*, 214113.
(23) Woodward, D. I.; Reaney, I. M. *J. Phys.: Condens. Matter* **2004**, *16*, 8823.
(24) Correas, C.; Jiménez, R.; Hungría, T.; Amorín, H.; Ricote, J.; Vila, E.; Algueró, M.; Castro, A.; Galy. J. Ceram. Trans., in press.

Structural Characterization. The evolution of the reactions was followed by X-ray powder diffraction (XRD), at room temperature, on a Philips X'Pert diffractometer, fitted with a Ge(111) incident beam monochromator of the Johansson symmetric type, using Cu $K_{\alpha 1}$ radiation (λ = 1.5406 Å). Data were recorded between 5° and 60° (2θ), with 2θ increments of 0.04° and counting time of 1 s per step. For the determination of the lattice parameters, patterns from 20° to 96° (2θ) were measured at room temperature in the same Philips X'Pert diffractometer. Data were taken at steps of 0.01° for 10 s. The flat sample was spun around its normal at about 2 Hz. A small amount of NIST Si standard (Standard Reference Material 640b, a = 5.430940 Å for the wavelength quoted above), mixed with the sample material, was used for calibration purposes.

In order to verify the structural evolution with temperature of each phase, mainly if the ferro-paraelectric transition occurred, high-resolution XRD patterns of three representative materials, 0.3BM−PT (tetragonal), 0.4BM−PT (MPB tetragonal-pseudocubic), and 0.5BM−PT (pseudocubic), were recorded in a Synchrotron ion beamline 2 at the European Synchrotron Radiation Facility (ESRF) in Grenoble, France. A Si (1 1 1) channel cut monochromator and a Ge (2 2 0) analyzer crystal were used to give a wavelength of 1.03283415 Å, using a beam energy of E = 12 keV. The XRD data were collected, at room temperature and 773 K (temperature above the ferroelectric transition of $PbTiO_3$), by step scanning from 12° to 55° (2θ) with a sampling interval of 0.02° taking 2 s per step.

The determination of the experimental density of the new isolated phases was carried out with an Accupyc 1330 pycnometer using the helium displacement technique.

Morphological characteristics of both powdered and ceramic samples were elucidated by scanning electron microscopy (SEM) and transmission electron microscopy (TEM). TEM experiments were carried out in a CM20 FEG Philips microscope working at 200 kV. For these studies, powdered samples were crushed in an agate mortar and suspended in *n*-butanol. After ultrasonic dispersion, a droplet was deposited on a copper grid supporting a perforated carbon film. SEM characterization was performed on fracture surfaces of the sintered ceramics, with a JEOL JSM-6490 microscope working at 30 kV.

Thermal Behavior and Electrical and Mechanoelastic Characterization. The thermal behavior of the different samples was studied by thermogravimetric (TG) and differential thermal analysis (DTA). The DTA and TG measurements were carried out in air, from room temperature to 923 K, using a Seiko 320 instrument, with α-Al_2O_3 as the inert reference material. The heating−cooling rates were 10 K·min^{-1}, and the quantity of sample used was about 40 mg.

Ag electrodes were painted (Dupont 7095) on the major faces of thinned ceramic discs and sintered at 923 K for electrical characterization. The dependence of the dielectric permittivity on temperature was firstly measured above room temperature (RT) up to 800 K with a HP4284A precision LCR (Inductance-Capacitance-Resistance) meter. Measurements were dynamically carried out during a heating−cooling cycle at ±2K·min^{-1} rate at 9 frequencies between 100 Hz and 1 MHz. Secondly, the permittivity was measured below RT down to 77 K with the same LCR meter. In this case, measurements were dynamically carried out during heating from the liquid nitrogen temperature at +1.5 K·min^{-1}, also at 9 frequencies between 100 Hz and 1 MHz.

The low frequency Young's modulus and mechanical losses were measured as a function of temperature by dynamical mechanical analysis in the three-point bending configuration with a Perkin Elmer DMA7 apparatus. A stress sine wave of 8.5 MPa amplitude, superimposed on a static stress of 10 MPa, was applied to ceramic bars of 12 × 2 × 0.35 mm^3 dimensions. Measurements were dynamically accomplished at a single frequency of 1 Hz during a cooling−heating cycle, from 723 to 77 K and back to high temperature with ±2K·min^{-1} rates.

Magnetic Characterization. For the magnetic measurements, a SQUID magnetometer MPMS-XL Quantum Design was used. It was calibrated with a Pd standard. The superconducting magnet is able to produce magnetic fields up to ±50 kOe, with resolution of 0.1 Oe for applied field lower than 5000 Oe and 1 Oe for H > 5000 Oe. Thermal stability is about ±0.01K, and sensitivity in magnetic moment determination is around ~10^{-8} emu·g^{-1}. The quantity of each sample used was around 200−400 mg for the magnetic susceptibility measurements between 1.9 K and room temperature at 1 kOe under both zero field cooling (ZFC) and field cooling (FC) conditions. Isothermal magnetization measurements were performed up to 50 kOe at different temperatures.

Results and Discussion

The synthesis of xBM−PT occurs via the formation of intermediate products with very low particle size, which evolve to perovskite phases at about 1173 K. However, a final thermal treatment at 1273 K for $x \leq 0.6$ and 1233 K for $0.6 < x \leq 0.8$ was needed in order to isolate very crystalline samples. Figure 1a shows the final XRD patterns of the prepared compositions. Single and well crystallized phases were isolated for x values ranging between 0 and 0.74. Three different structural regions can be distinguished: the first one, for $0 \leq x < 0.36$, corresponds to the tetragonal symmetry, isostructural with $PbTiO_3$; in the second region, located between x = 0.36 and x = 0.44, the coexistence of tetragonal and pseudocubic symmetries can be easily viewed, that is the existence of a morphotropic phase boundary (Figure 1b); the third region covers from x = 0.46 to x = 0.8, exhibiting a single pseudocubic symmetry. Further away, for $x > 0.74$, small quantities of secondary phases were detected together with the pseudocubic one.

These results contrast with those reported by Woodward et al,[23] who state the occurrence of an abrupt symmetry change from tetragonal to pseudocubic, between $0.4 < x < 0.5$, perhaps with some asymmetry detected in the cubic {100} and {110} diffraction lines of x = 0.4 and suggest it to result in the frustration of the polar long range order and the formation of a relaxor state.

Classically, morphotropic phase boundary (MPB) in $BiBO_3$−$PbTiO_3$ systems occur at quite narrow composition limits that require accurate synthesis processes to be detected. The wet-chemistry method used in the present work allows fine and very homogeneous powder to be obtained (Figure 2a), owing to the fact that the mixing of the reactants occur at almost atomic level scale; therefore, the reaction pathway can be better controlled than that of solid-state reaction route.[23] This fact, together with the study of the adequate compositions, has led the morphotropic phase boundary to be detected.

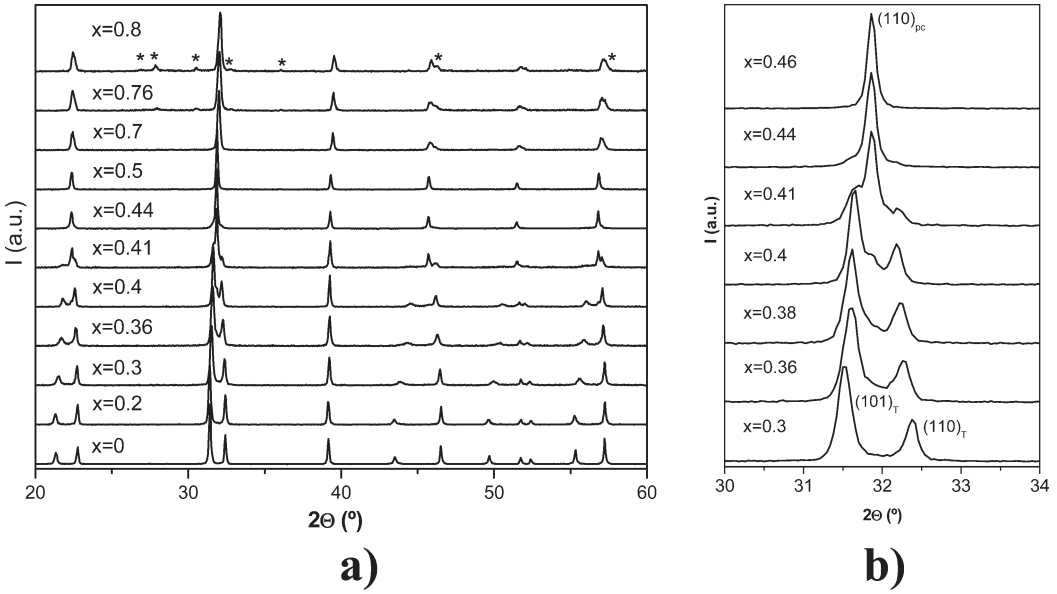

Figure 1. (a) X-ray diffraction patterns of xBM−PT phases for the whole solid solution; (b) morphotropic phase boundary evidence in $0.3 < x < 0.46$. (∗, unidentified phases).

This morphotropic phase boundary is related to a critical value of the tolerance factor (t) of perovskites[25] for this system t is given by

$$t = \frac{\mathrm{Ra} + \mathrm{Ro}}{\sqrt{2}(\mathrm{Rb} + \mathrm{Ro})}$$

where Ra and Rb are the average ionic radii of A and B cations, in XII and VI coordination, respectively, and Ro is the anionic radius of oxygen in VI coordination. In fact, for this system, the tetragonal form is the only stable for $x < 0.36$, that is $t \geq 0.99$, while the single pseudocubic perovskite is the only detected phase from $x = 0.46$ or $t \leq 0.98$. However, the presence of the MPB is limited to $t \approx 0.99$ and $0.36 \leq x \leq 0.44$, which seems to be the critical value for this system.

Unit-cell parameters have been refined by a least-square method for all synthesized phases, including those of tetragonal and pseudocubic forms in the MPB region; Figure 3 shows their evolution versus composition. When bismuth/manganese substitution for lead/titanium is low, up to $x < 0.2$, the network remains almost unchanged with the tetragonal distortion c/a ≈ 1.07 and then subsequently contracts as x increases up to $x = 0.44$, the tetragonal distortion diminishing down to c/a ≈ 1.03. Moreover, the pseudocubic phase appears at $x = 0.36$ and its reticular parameter, a_{PC}, and so, the volume cell monotonically diminishes when x increases, up to $x = 0.8$, even if small quantities of unidentified diffraction lines are present. It is worth noting the considerable difference between cell parameters of both tetragonal and pseudocubic phases, occurring in the MPB region.

The morphology of the synthesized phases has been studied by transmission and scanning electron microscopy. As an example, Figure 2 depicts the TEM micrograph of a 0.3BM−PT powdered sample, obtained at 1173 K, as well as the SEM image and grain-size distribution of the corresponding ceramic, sintered at 1273 K. While the powdered perovskites are constituted by submicronic agglomerates of small-sized crystals (Figure 2a), the sintered ceramics exhibit an almost homogeneous grain-size distribution, with average size of 10 μm (Figure 2b,c).

In order to study the possible ferroelectric character of these materials, several measurements have been carried out. Firstly, their thermal behavior has been followed by differential thermal analysis. Figure 4 shows the heating−cooling cycles for xBM−PT samples up to $x = 0.25$. A unique reversible endothermic effect was observed for all compositions. Such effect is very intense and sharp for $PbTiO_3$ ($x = 0$), becoming less pronounced and broad as x increases. In the case of $PbTiO_3$, the feature is well known to be associated with the ferroelectric first-order transition that this material undergoes at Tc ≈ 763 K between the tetragonal and cubic phases.[26,27] Therefore, the effects detected in DTA curves for the xBM−PT system can be also attributed to their ferro-paraelectric transition. A clear hysteretic behavior was observed in heating−cooling cycles, which transitions occur at high temperatures on heating.

The tricritical point is defined as the composition of a solid solution at which a first- becomes a second-order transition.[28] This point was found to be close to compositions with tolerance factors $t \approx 1.0$, for several perovskite solid solutions, $PbTiO_3$ derived, for example: $BiMg_{3/4}W_{1/4}O_3$−$PbTiO_3$,[28] $PbZrO_3$−$PbTiO_3$,[29] or $BiScO_3$− $PbTiO_3$.[30]

(25) Goldschmidt, V. M. *Geochemisca Veterlun*; Norske Videnkap: Oslo, 1927.

(26) Burns, G.; Scott, B. A. *Phys. Rev. B* **1973**, *7*, 3088.
(27) Sani, A.; Hanfland, M.; Levy, D. *J. Solid State Chem.* **2002**, *167*, 446.
(28) Stringer, C. J.; Eitel, R. E.; Shrout, T. R.; Randall, C. A.; Reaney, I. M. *J. Appl. Phys.* **2005**, *97*, 024101.
(29) Rossetti, G. A.; Navrotsky, A. *J. Solid State Chem.* **1999**, *144*, 188.
(30) Eitel, R.E. PhD, The Pennsylvania State University, University Park, PA, **2003**.

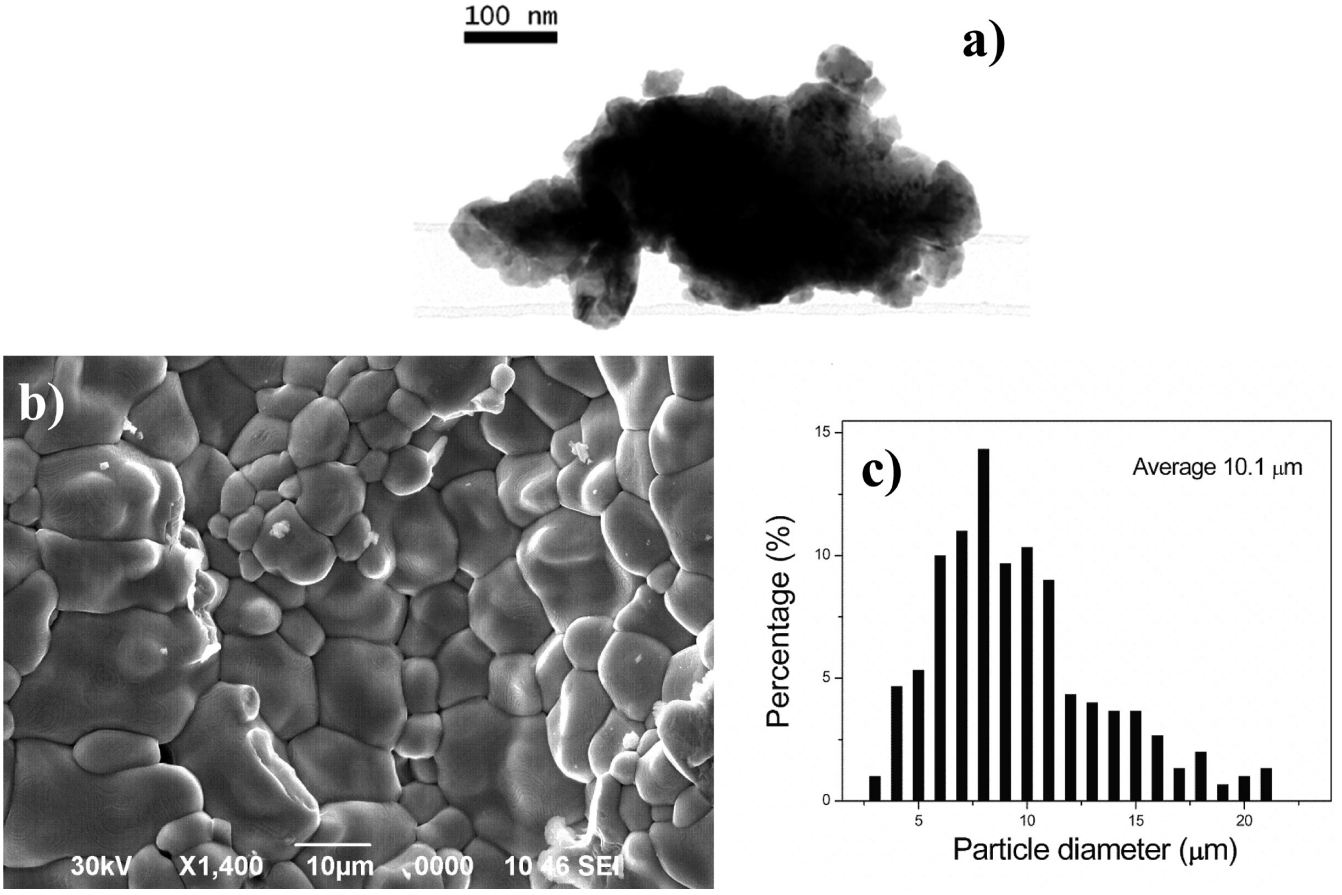

Figure 2. (a) TEM micrograph of 0.3BM−PT powder obtained at 1173 K; (b) SEM image of 0.3BM−PT ceramic sintered at 1273 K; (c) grain-size distribution in 0.3BM−PT ceramic.

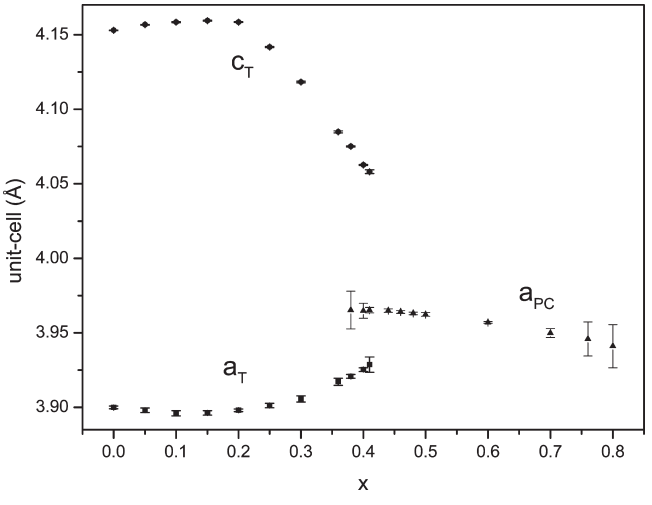

Figure 3. Evolution of the unit-cell parameters in the system xBM−PT. (a_T and c_T, a and c parameters of tetragonal perovskite; a_{PC}, a axe of pseudocubic perovskite. Standard deviations are represented as 3σ.)

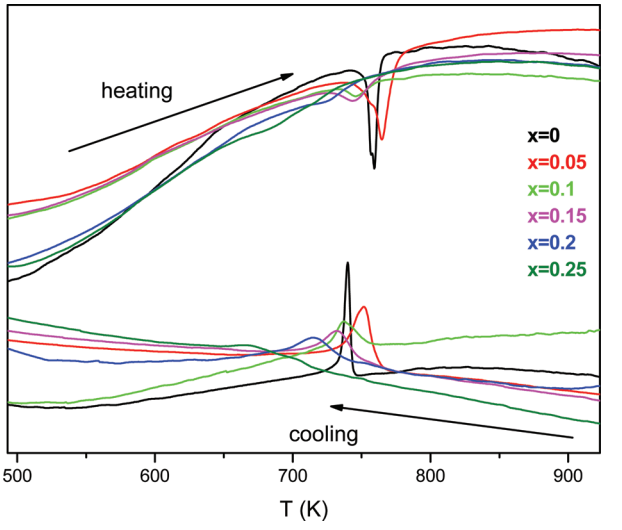

Figure 4. Differential thermal analysis curves on heating−cooling cycles for selected xBM−PT phases.

The same trend seems to occur in xBM−PT, where the transition peak vanishes between $x = 0.25$ ($t = 1.001$) and $x = 0.3$ ($t = 0.997$), in the DTA curves (Figure 4), while the room temperature phase is still tetragonal for these compositions. Hence, the tricritical point of xBM−PT is located around $x = 0.25$, and a second-order transition can be supposed for $x \geq 0.3$.

The occurrence of the ferroelectric transition up to $x = 0.25$ was confirmed by the electrical measurements. The temperature and frequency dependences of the dielectric permittivity and losses for $x = 0.15$ are shown in Figure 5 as an example. A reversible, nondispersive dielectric anomaly is observed at temperatures of 742 and 738 K on heating and cooling, respectively, which are in good

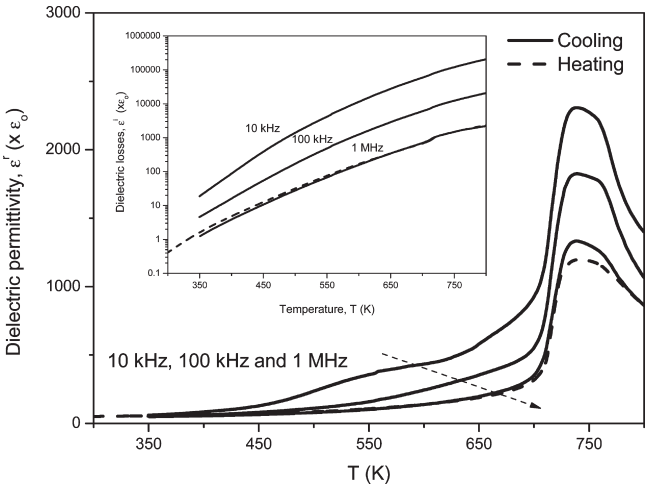

Figure 5. Temperature dependence of permittivity for 0.15BM−PT at several frequencies. Dielectric losses are shown in the inset.

agreement with the temperature of the endothermic process in the DTA measurements. Note also the presence of a strong dielectric dispersion all across the temperature range investigated, which is most probably associated with the presence of electrical conductivity, as indicated by the dielectric losses shown in the inset. This non-negligible conductivity prevented ferroelectric hysteresis loop measurements at room temperature.

No dielectric anomaly associated with the ferroelectric transition was found for $x > 0.25$, in spite of phases being tetragonal up to $x = 0.36$. This is illustrated in Figure 6a, where the temperature and frequency dependences of the dielectric permittivity and losses are shown for $x = 0.3$. A step-like increase with temperature and huge dispersion are observed, which are typical of Maxwell-Wagner type relaxation caused by the activation and movement of free charge carriers. Perovskite is pseudocubic for $x > 0.44$ at room temperature, so the ferroelectric transition must occur, if it takes place, below room temperature. Dielectric permittivity and losses for $x = 0.5$ are shown in Figure 6b down to 77 K. Again, no dielectric anomaly is observed but a Maxwell-Wagner type relaxation.

The electrical response of these samples is, thus, dominated by conduction effects, and a different analysis is needed. The admittance spectra for the sample with $x = 0.3$ is shown in Figure 7a at different temperatures. Note the presence of a frequency independent region associated with a long-range conductivity that is blocked at lower frequencies. Similar results are obtained for $x = 0.50$. Conductivity values in this region have been evaluated as a function of temperature, and Arrhenius plots are shown in Figure 7b. Activation energies of 0.44 eV and 0.33 eV are obtained for $x = 0.3$ and 0.5, respectively, which are slightly smaller than that of conduction for the $BiFeO_3$ phase (0.6 eV), above the Néel temperature. In this latter case, the conduction mechanism has been proposed to be the hopping of valence electrons between Fe^{2+} and Fe^{3+} cations in octahedral sites associated with oxygen vacancies.[31]

(31) Bhattacharjee, S.; Pandey, V.; Kotnala, R. K.; Pandey, D. *Appl. Phys. Lett.* **2009**, *94*, 012906.

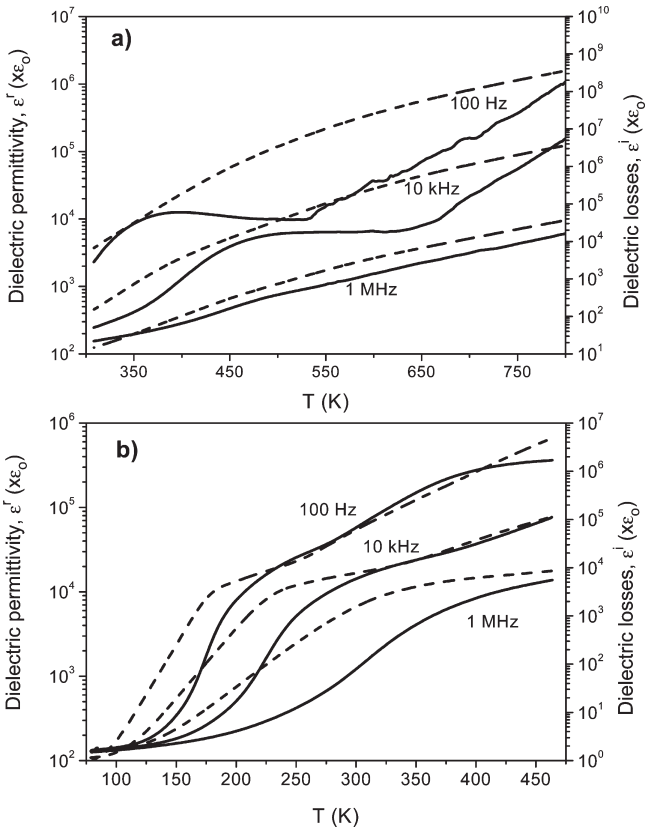

Figure 6. Temperature dependences of the dielectric permittivity and losses for (a) 0.3BM−PT and (b) 0.5BM−PT.

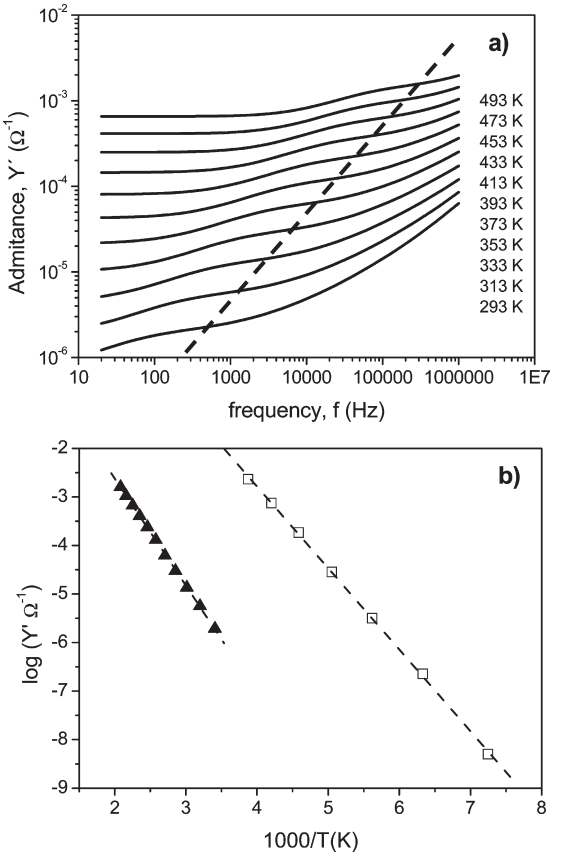

Figure 7. (a) Admittance spectra for 0.3BM−PT at several temperatures. (b) Arrhenius plots for the conductivity of xBM−PT with $x = 0.3$ and 0.5. (▲, $x = 0.3$; □, $x = 0.5$; ---, linear fits).

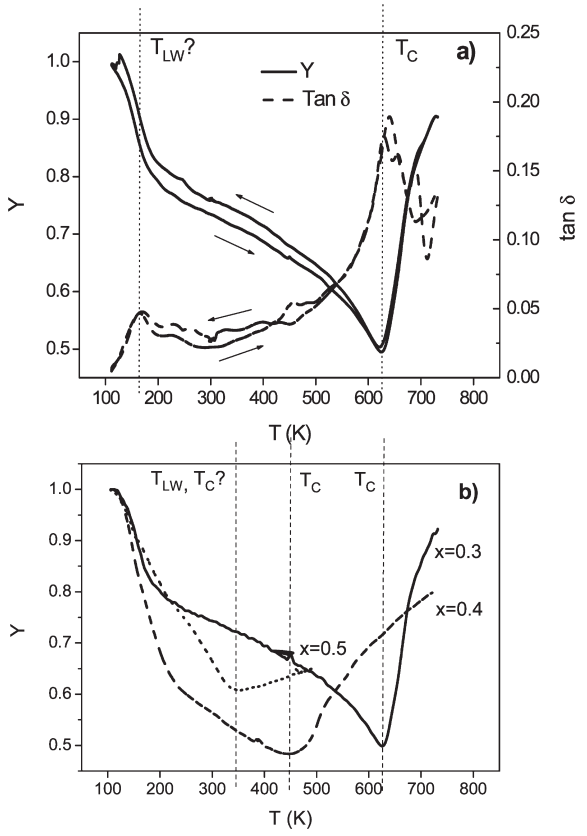

Figure 8. (a) Young's modulus and mechanical losses for 0.3BM−PT measured during a cooling−heating cycle; (b) Young's modulus for xBT−PT with x = 0.3, 0.4, and 0.5 measured during cooling (f = 1 Hz). Ferroelectric transitions are indicated (T_C), along with the low temperature hardening process (T_{LW}). (Y, normalized Young's modulus; tan δ, mechanical loss tangent.)

A similar mechanism might be active in xBM−PT materials involving Mn^{2+} and Mn^{3+}.

Dynamical mechanical analysis is a powerful alternative technique for studying ferroelectric transitions that present electromechanical coupling (they are also improper ferroelastic transitions), specially useful when conduction phenomena mask the dielectric anomalies,[32] as it is the case for xBM−PT with $x > 0.25$. The low frequency Young modulus and mechanical losses as a function of temperature are shown in Figure 8a for x = 0.3. The reversible elastic anomaly at T = 626 and 620 K on heating and cooling, respectively, which has associated a maximum of mechanical losses is typical of a ferroelectric phase transition.[33] This is consistent with this composition being tetragonal at room temperature.

Measurements were also carried out with samples of x = 0.4 and x = 0.5, and results are shown in Figure 8b along with those for x = 0.3. The elastic anomaly associated with the ferroelectric transition is shifted towards lower temperatures with x, down to 448 K for x = 0.4. For x = 0.5, there is still a minimum in Y at 328 K, but its shape is not that of an elastic anomaly associated with a ferroelectric transition, and the perovskite is pseudocubic at room temperature.

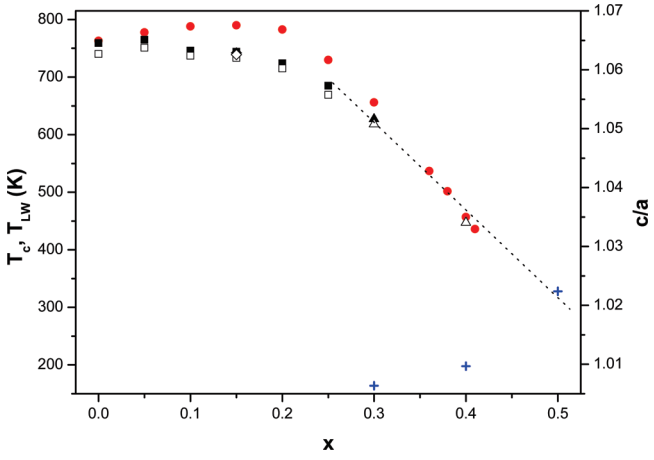

Figure 9. Curie (T_C) and hardening temperature (T_{LW}) measured on heating and cooling and tetragonal distortion (c/a) versus composition in xBM−PT system. (■, Tc from DTA measures on heating; □, Tc from DTA measures on cooling; ▲, Tc from DMA measures on heating; Δ, Tc from DMA measures on cooling; ♦, Tc from dielectric measures on heating; ◊, Tc from dielectric measures on cooling; blue +, T_{LW}; red ●, c/a.)

There is a second, also reversible, low temperature anomaly for x = 0.3 and 0.4, at which a sharp hardening occurs along with a maximum in losses, below which the losses vanish. This hardening takes place at 167 and 198 K for x = 0.3 and 0.4, and it is most probably associated with the disappearance of ferroelasticity, so it might indicate a transition to a lower symmetry, nonpolar phase.

This second anomaly shifts towards higher temperatures with x, so it is tempting to propose that the minimum in Young's modulus for x = 0.5 results in the occurrence of the hardening before the ferroelectric transition takes place. A similar elastic anomaly has been reported for $BiFeO_3$ and proposed to be a magnetic transition with magnetoelastic coupling.[34] Nevertheless, $BiMnO_3$ has the ferromagnetic transition at 100 K, which is well below the temperatures at which the elastic anomalies are observed.

Therefore, the combination of DTA, electrical, and mechanical measurements has allowed us to follow the ferroelectric phase transition up to x = 0.4. It is worth comparing the evolution of both tetragonal distortion and Curie temperatures, measured by different techniques (Figure 9), with composition in the xBM−PT system. As it can be observed in Figure 9, both parameters follow the same trend; they do not appreciable change up to x = 0.2 and then start to diminish approximately at the tricritical point (x = 0.25). That is to say, when the first-order transition turns into second order, from x = 0.25, tetragonality and Tc quickly fall down to x = 0.4, in coincidence with the end of MPB. The temperature of the low temperature hardening (disappearance of ferroelasticity) is also shown in the Figure 9. This temperature increases with x, and it is above room temperature for x = 0.5. From these results, it is quite predictable, the

(32) Jiménez, R.; Castro, A.; Jiménez, B. *Appl. Phys. Lett.* **2003**, *83*, 3350.
(33) Jiménez, B.; Vicente, J. M. *J. Phys. D: Appl. Phys.* **1998**, *31*, 130.
(34) Redfern, S. A. T.; Wang, C.; Hong, J. W.; Catalan, G.; Scott, J. F. *J. Phys.: Condens. Matter* **2008**, *20*, 452205.

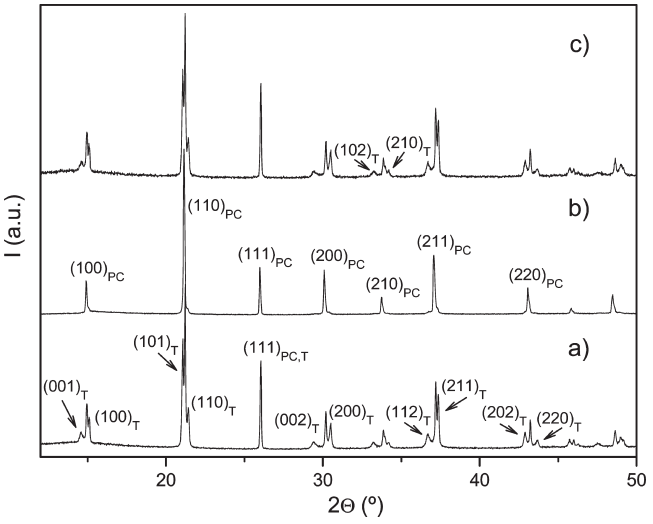

Figure 10. Synchrotron XRD patterns of 0.4 $BiMnO_3$−0.6 $PbTiO_3$ recorded at room temperature (a), at 773 K (b), and at room temperature on cooling (c). (T, tetragonal, PC, pseudocubic.)

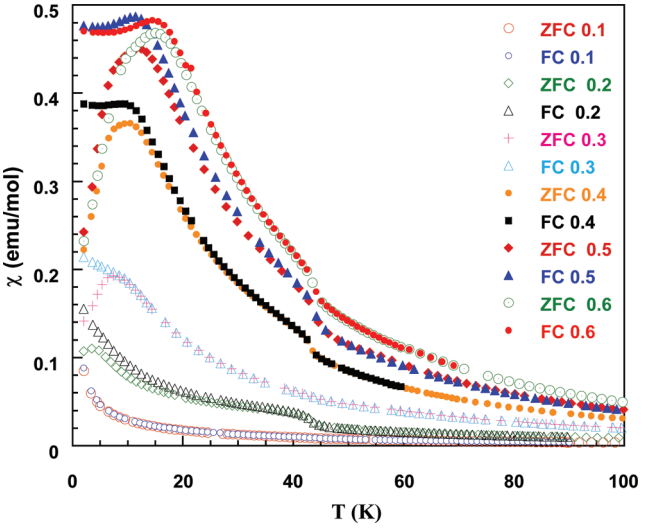

Figure 11. Temperature dependence of the molar magnetic susceptibility at low temperature in xBM−PT samples for $0.1 \leq x \leq 0.6$ measured at applied field $H = 1000$ Oe. ZFC and FC measurements for each composition. Symbols label in the inset.

disappearance of ferroelectricity in the xBM−PT system beyond the MPB region.

With the aim to study the structural evolution arising in the ferro-paraelectric transition, high-resolution X-ray synchrotron diffraction patterns, of three representative compositions in the xBM−PT system, have been recorded in the SpLine ESRF of Grenoble (France), at room and high temperatures (773 K), below and above the transition. The selected compositions were $x = 0.3$, tetragonal and ferroelectric; $x = 0.4$, MPB region and also ferroelectric; and $x = 0.5$, pseudocubic with no ferroelectric transition detected down to 77 K. Results corresponding to $x = 0.4$ are depicted in Figure 10. Again, this composition proves itself to belong, at room temperature, to the MPB region, with very well differenced tetragonal and pseudocubic diffraction lines. At temperatures higher than Tc, the tetragonal phase disappears and only the pseudocubic diffraction lines were present. On cooling, the transition seems to be reversible and the XRD pattern goes back to the initial room-temperature one. Equivalent results were obtained for $x = 0.3$ and $x = 0.5$, with no transition detected for the last one and a clean tetragonal−pseudocubic−tetragonal transition viewed for $x = 0.3$. These results further support the ferroelectric character of $x \leq 0.44$ phases, while those with $x > 0.44$ would be paraelectric, in such a way that the morphotropic region of this system would be of tetragonal, ferroelectric−pseudocubic, paraelectric type.

In order to study the magnetic properties of these materials, we have performed for the first time bulk magnetic measurements of the powder samples $x BiMnO_3$−$(1-x)\,PbTiO_3$ with $x = 0.1, 0.2, 0.3, 0.4, 0.5$, and 0.6. The dependence of the magnetic susceptibility $\chi = M/H$ with temperature in the range 300−2 K shows the existence of cooperative magnetic interactions at low temperature, presumably with finite correlation length. A strong upturn of χ versus T is observed for almost any composition

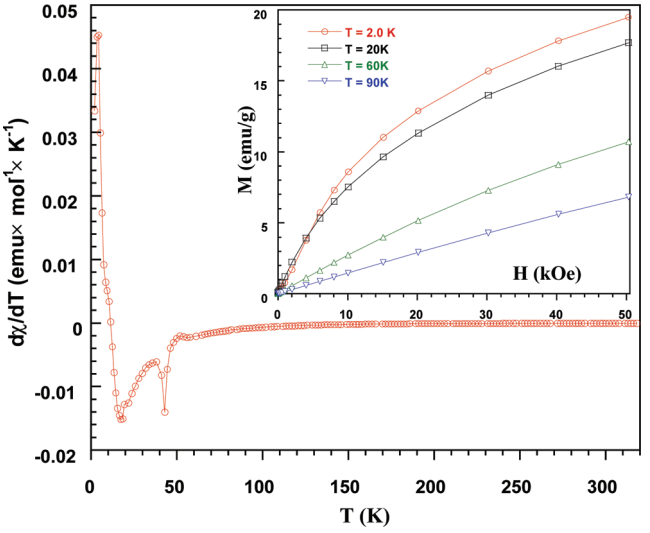

Figure 12. Magnetic susceptibility derivative versus temperature for 0.5BM−PT in temperature range from 1.9 to 320 K. Magnetization isotherms at the indicated temperatures versus applied magnetic field H are shown in the inset.

around $T < 50$ K, pointing to the somehow ferromagnetic nature of the interactions.

Figure 11 shows the dc molar magnetic susceptibility vs temperature in this range, both at zero field cooling (ZFC) and field cooling (FC). ZFC measurements show the existence of broad maxima at the temperatures indicated in Table 1. The onset of these magnetic phase transitions is better seen in the derivatives $d\chi/dT$ versus T; temperatures of peak positions (minima) are shown in Table 1. As an example, Figure 12 plots $d\chi/dT$ versus T for $x = 0.5$. It is worth mentioning that the higher x in xBM−PT, the higher temperature of the maximum in χ. This behavior reflects that increasing the chemical dilution of the magnetic Mn^{3+} sublattice decreases the magnetic interactions which finally vanish for $x = 0.1$. In a similar way, it has been observed that T_N decreases with

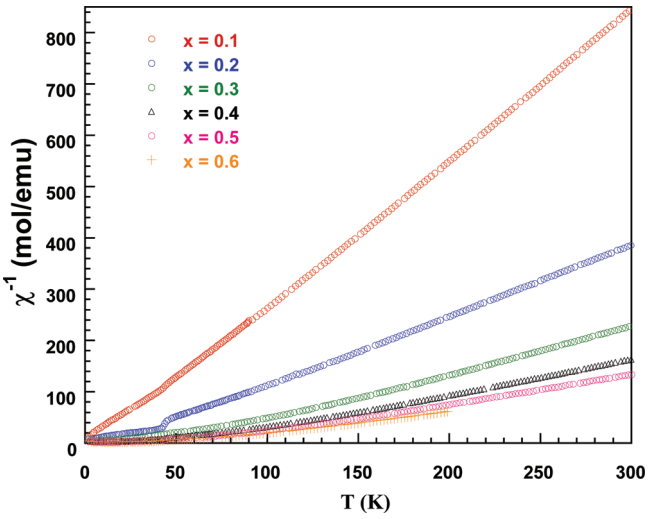

Figure 13. Variation of the molar magnetic reciprocal susceptibility in the 300−2 K temperature range for xBM−PT samples with $0.1 \leq x \leq 0.6$ measured under applied field $H = 1$ kOe after ZFC.

Table 1. Effective Paramagnetic Moment Obtained For Mn^{3+} in $x BiMnO_3-(1-x)PbTiO_3$, Weiss Constants, and Temperature of the Maximum in the Susceptibility

x	$\mu_{eff}Mn^{3+}$ (μ_B)	θ (K)	$T_{\chi Max}$ (K)	$T_{d\chi/dT}$ (K)
0.1	5.21	13.6		
0.2	5.36	22.7	3.5	6.0
0.3	5.32	58.7	7.4	12.4
0.4	5.37	65.3	10.4	15.5
0.5	5.25	69.8	12.4	17.5
0.6	5.43	62.6	15.0	21.0

Fe^{3+} dilution in the antiferromagnetic $(1-x)$ $BiFeO_3-x$ $PbTiO_3$ solid solution.[35]

Reciprocal susceptibility χ^{-1} versus T follows a Curie−Weiss law in a wide T range and deviates from linear behavior at low temperatures due to the interactions (see Figure 13). The effective magnetic moment obtained from the fitting of CW law in the paramagnetic region above $T > 150$ K amounts around 5.3 μ_B somewhat slightly higher than the expected for $Mn^{3+}d^4$ in high spin state if spin-only contribution is taken into account, i.e., $\mu_S = 4.90\ \mu_B$. We mention that if the orbital angular contribution is not quenched it turns to $\mu_{S+L} = 5.48\ \mu_B$ and remark that for $Mn^{2+}d^5$ $\mu_{eff} = \mu_S = 5.92\ \mu_B$. We cannot totally rule out the existence of a small amount of spurious phase (< 2% weight) not detected in the X-ray diffraction patterns, for example Mn_2O_3 (ferromagnet) or $Bi_2Mn_4O_{10}$ (antiferromagnet), but it does not mask the general behaviour of the bulk.

The obtained parameters are shown in Table 1 together with the Weiss constant θ; their positive values also point to the predominantly ferromagnetic character of the interactions. Inset of Figure 12 displays magnetization curves versus applied field H for the $x = 0.5$ sample, showing a linear behavior above the transition temperature and field induced ferromagnetic interactions at lower temperature. However, saturation is not reached up to $H = 50$ kOe.

On the other hand, FC measurements do not show net maxima but a further broadening at lower temperature. Irreversibility is observed between ZFC and FC χ at low temperature merging below $T = 50$ K. These properties could be due to spin-glass or cluster-glass behavior rather than whole long range ferromagnetic ordering. The chemical dilution of the Mn^{3+} magnetic sublattice by nonmagnetic cations supports this assumption. It should be noted that $BiMnO_3$ is ferromagnetic with Curie temperature $T_C \approx 100$ K,[36,37] orbital ordering has been invoked to explain the superexchange interactions through $Mn^{3+}-O^{2+}-Mn^{3+}$ bonds; however, superexchange pathways involving nonmagnetic cations of the type $Mn^{3+}-O^{2+}-Ti^{4+}-O^{2+}-Mn^{3+}$ and chemical disorder could lead to frustration and competing interactions in such a way that avoids a full long range magnetic order in the system. Also, in the related system, $BiMn_{1-x}Sc_xO_3$ spin-glass behavior has been observed.[38] To clarify this aspect, alternating current (ac) susceptibility measurements are in progress as they should show different dependence with field and frequency whether the system behaves as ferromagnet or spin-glass. In order to fully characterize the magnetic and crystal structures of the system, neutron diffraction experiments will be carried out taking into account that long range antiferro- or ferromagnetic order gives rise to magnetic scattering condensed in Bragg reflections contrary to spin-glass behavior.

In summary, from the structural characterization, it can be concluded that the xBM−PT system forms a solid solution, exhibiting different symmetries as a function of bismuth/manganese for lead/titanium substitutions (x): tetragonal, $0 \leq x < 0.36$; morphotropic phase boundary between tetragonal and pseudocubic symmetries, $0.36 \leq x \leq 0.44$; and pseudocubic, $0.44 < x \leq 0.8$. The ferroelectric phase transition has been followed by a combination of techniques up to $x = 0.4$, including DTA, electrical, and mechanoelastic measurements. For $x \geq 0.5$, the temperature dependence of the Young′s modulus strongly suggests that the ferroelectric phase transition does not occur, but instead, there is a transition to a nonferroelastic phase. This can raise doubts about the ferroelectric nature of $BiMnO_3$, in good agreement with recent results reported by Baettig et al.[39] Furthermore, the magnetic measurements confirm the existence of magnetic interactions in this system; however, the observed critical temperatures of the transitions fall quite below the hardening temperatures observed in Young′s modulus measurements, which prevents us to invoke for magnetostriction effects coupling magnetic and elastic order parameters.

(35) Zhu, W. M.; Guo, H. Y.; Ye, Z. G. *Phys. Rev. B* **2008**, *78*, 014401.
(36) Atou, T.; Chiba, H.; Ohoyama, K.; Yamaguchi, Y.; Syono, Y. *J. Solid State Chem.* **1999**, *145*, 639.
(37) Montanari, E.; Calestani, G.; Righi, L.; Gilioli, E.; Bolzoni, F.; Knight, K. S.; Radaelli, P. G. Phys. Rev. B **2007**, *75*, 220101(R).
(38) Belik, A. A.; Yokosawa, T.; Kimoto, K.; Matsui, Y.; Takayama-Muromachi, E. *Chem. Mater.* **2007**, *19*, 1679.
(39) Baettic, P.; Seshadri, R.; Spaldin, N. A. *J. Am. Chem. Soc.* **2007**, *129*, 9854.

Acknowledgment. We thank the Spanish MICINN for financial support (projects MAT2007-61884 and MAT2008-02003/NAN) and SpLine (Spanish CRG) and ESRF. We also thank Ms. I. Martínez for her valuable help in sample preparation and X-ray and DTA characterization. T.H. is indebted to the CSIC (MICINN) of Spain for the "Junta de Ampliación de Estudios" contract (Ref JAEDOC082). J.H.-V. thanks the MICINN for funding through the "Ramón y Cajal" programme.